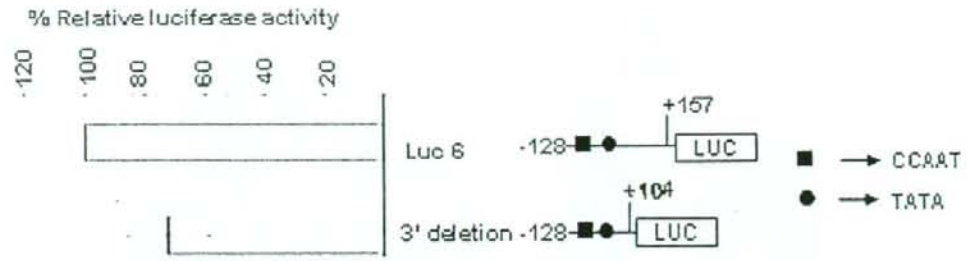

Figure 11
Luciferase analysis of 3' -deleted Luc 6 constructs as compared to wild type Luc 6 construct showing ~ 28% reduction of reporter activity. All transfections were repeated in duplicates and the results are expressed as the mean of two different experiments ± S.D. On right, a schematic representation of 3' deleted luciferase construct used for transfection is depicted along with wild Luc 6. Approximate locations of transcription factor binding sites are shown.

glycerol at room temperature for 30 minutes. Subsequent to binding reaction 7.5 mM $MgCl_2$ and 5 mM $CaCl_2$ were added and samples were incubated at room temperature with DNase I (0.25 U, Roche, USA) for 60 s. Ten to twenty folds less DNase I was used for control experiments without nuclear extracts. DNase I enzyme digestion was stopped by the addition of an equal volume of 1% SDS, 20 mM EDTA, 400 mM NaCl, 100 μg/ml yeast tRNA and 200 μg/ml proteinase K. Following incubation at 45 °C for 60 minutes, samples were extracted twice with phenol/chloroform, precipitated with ethanol and electrophoresed on 6% polyacrylamide sequencing gel. After electrophoresis, gels were dried on Whatman filter paper and autoradiographed. Primers used for generating end labeled DNA fragments for footprinting of the region -513/-352 bp are: 5' -GCCTCATGCAAGGAAGCAAG-3' SS and 5' -GATAATGGCAGGTATGAGGG-3' AS. Primers used for footprinting from -2750 bp to -777 bp are shown in table 1.

Electrophoretic mobility shift assay (EMSA)

Oligonucleotides (both strands) corresponding to identified DNase I protected sites (table 2, 3, 5 and 6) were synthesized. For each site, one strand was end-labeled with [γ-^{32}P] ATP using T_4 polynucleotide kinase and annealed to its complementary unlabeled strand. Nuclear extracts (4–6 μg) were incubated with 20 fmoles of radiolabeled oligonucleotide duplex in 30 μl reaction containing 10 mM Tris-HCl (pH 7.5), 50 mM NaCl, 1 mM EDTA, 1 mM DTT, 5 % glycerol and 1.0 μg poly (dI-dC) for 20 minutes at room temperature. In competition experiments, 100-fold molar excess of unlabeled oligonucleotide duplexes were added during preincubation period. For antibody shift assay, C/EBPβ antibody (Santacruz, USA) was added after addition of nuclear extract and incubated at 4 °C for 10 min. Free DNA and protein bound DNA was separated on 5% non-denaturing polyacrylamide gel in 0.5 X Tris-boric acid-EDTA (TBE). After electrophoresis, gels were blotted onto filter paper, dried and autoradiographed.

Construction of 5' and 3' -serially deleted SMP30 fragments and it's cloning into pGL3-Basic vector

To construct 5' -serially deleted SMP30 fragments Luc-SMP-XhoI reverse primer and the forward primers as mentioned in table 4, containing Kpn1 sites were used. The PCR amplification was carried out using step cycles (94 °C for 30 s, 62 °C for 30 s, 72 °C for 30 s) for 35 cycles with a final extension at 72 °C for 10 minutes. Then the PCR products were purified using QIAquick Gel Extraction Kit (Qiagen, USA). The serially deleted fragments and pGL3-Basic vector were digested with KpnI and XhoI enzyme (MBI Fermentas). The digested 5' -serially deleted fragments were then ligated into restriction enzyme digested pGL3-Basic vector using DNA ligase (USB, USA). The cloned fragments were then confirmed by vector specific PCR using RV and GL2 primer, and also by sequencing.

Site-directed mutagenesis

Five to six bases of the transcription factor core binding site were mutated as shown in the table 5 (bases in small letter represents mutated base). For mutagenesis of transcription factors two sets of PCR were carried out using the following combination of primers: For Sp1: MutSp1 sense/Luc-SMP-XhoI antisense and Luc 5 sense/Mut Sp1 antisense; for C/EBP: Mut C/EBP sense/Luc-SMP-XhoI antisense and Luc 5 sense/Mut C/EBP antisense; for Mut Luc 3–1: Mut Luc3-1 sense/Luc-SMP-XhoI antisense and Luc-SMP-3 sense/Mut Luc 3–1 antisense; for Mut Luc 3–2: Mut Luc 3–2 sense/Luc-SMP-XhoI antisense and Luc-3 sense/Mut Luc 3–2 antisense; for Mut Luc 3–3: Mut Luc 3–

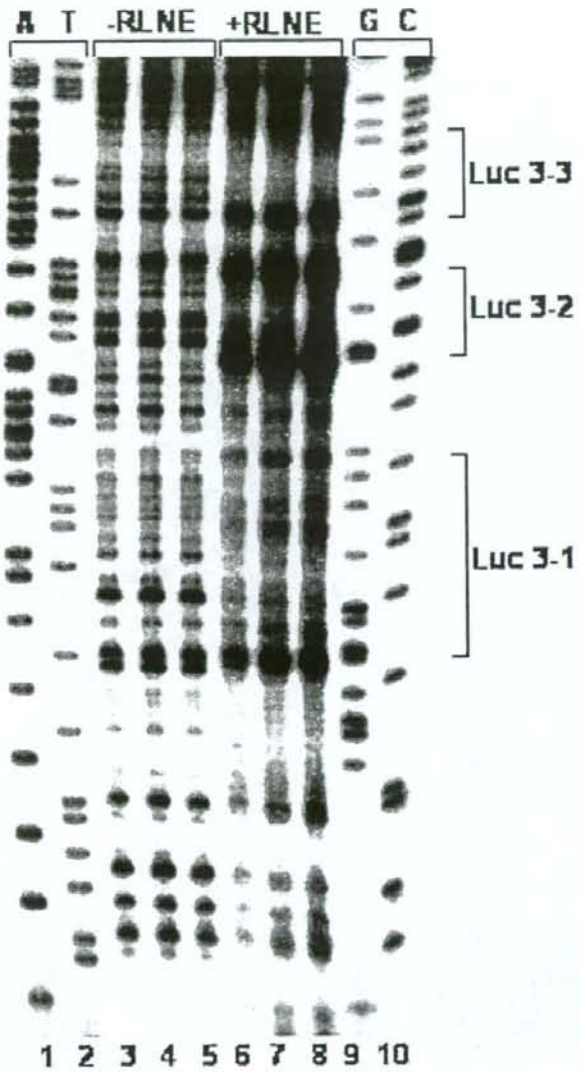

Figure 12
DNase I footprinting pattern of the repressor region (-513 to -352). *Lane 1,2 and 9,10* refer to sequencing reaction ladder obtained by taking the same labeled primer used in PCR for DNase I footprinting. *Lane 3,4,5* represent DNA treated with DNase I in absence of nuclear protein. *Lane 6,7,8* represent DNA treated with DNase I in presence of 50 μg rat liver nuclear extract (RLNE). The DNase I protected sites are marked on right site and the sequences are given in table 3. DNase I footprinting was carried out with fragments generated by labeled forward primer.

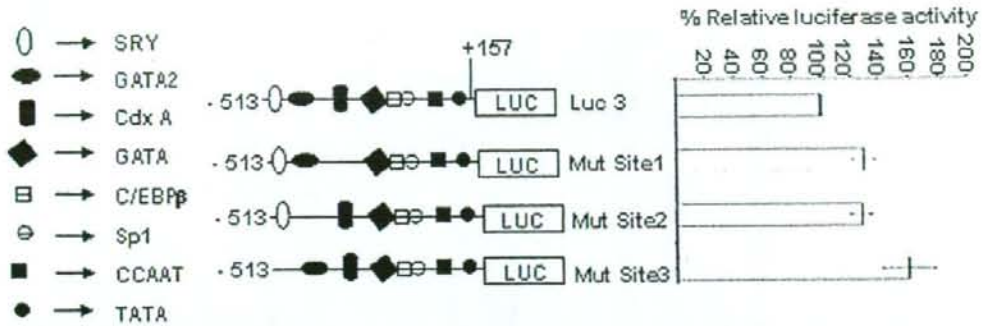

Figure 13
DNase I protected sites, Luc 3–1, Luc 3–2 and Luc 3–3 were mutated at their core binding sites. Reporter activity of the three mutated construct along with wild type Luc 3 construct is represented on the right site and the schematic representation of the mutated sites along with wild type Luc 3 on left site. All transfections were repeated in duplicates and the results are expressed as the mean of three different experiments ± S.D Approximate location of the transcription factor binding to wild type Luc 3 and site directed mutated construct are shown. Mutation of site 3 shows a significant (~59%) increase in luciferase activity as compared to wild type Luc3.

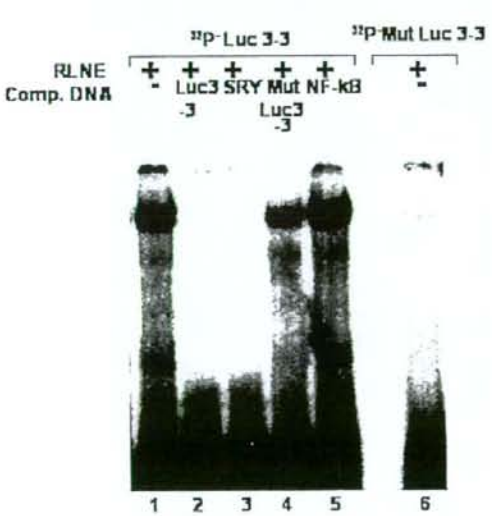

Figure 14
Electrophoretic mobility shift assay (EMSA) for site Luc 3–3 to confirm the binding of SRY transcription factor. *Lane 1*, labeled oligonucleotide duplex with 6 μg RLNE; *Lane 2–5*, 100 fold molar excess of unlabeled homologous self, SRY consensus, mutated Luc 3–3, nonspecific oligonucleotide duplex (NFkB). *Lane 6*, labeled Mut 3–3 oligonucleotide duplex with 6 μg RLNE.

Figure 15
EMSA for site Luc 3–2 to confirm the binding of GATA-2 transcription factor. *Lane 1*, labeled mutated oligonucleotide duplex with 6 μg RLNE; *Lane 2*, labeled oligonucleotide duplex with 6 μg RLNE; *lane3 -5*, 100 fold molar excess of unlabeled homologous self, GATA-2 consensus, and nonspecific (NFkB) oligonucleotide duplex (NFkB).

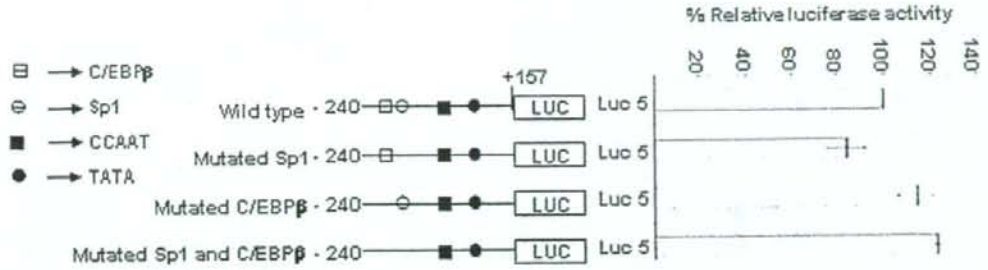

Figure 16

Reporter activity of site direct mutated Sp1, site direct mutated C/EBP and site direct mutated Sp1 and C/EBP sites reporter constructs along with wild type Luc 5 on right site and the schematic representation of the mutated Sp1 and C/EBP sites along with wild type Luc 5 sites on left site. All transfections were repeated in duplicates and the results are expressed as the mean of three different experiments ± S.D Approximate location of the transcription factor binding to wild type Luc 5 and site directed mutated construct are shown. A significant decrease (~16%) in reporter activity of mutated Sp1 construct is seen as compared with wild type Luc 5. There is no significant change in reporter activity with mutated C/EBP construct. Double mutation of Sp1 and C/EBP enhance the reporter activity by 23% as compared to wild type Luc 5.

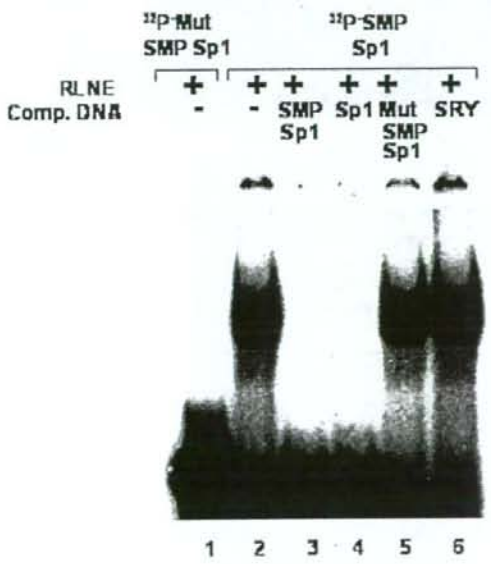

Figure 17

Electrophoretic mobility shift assay to confirm the binding of Sp1 transcription factor. *Lane 1*, labeled mutated SMP-Sp1 oligonucleotide duplex with 6 μg RLNE; *Lane 2–6*, labeled SMP-Sp1 oligonucleotide duplex with 6 μg RLNE; *Lane 3–6*, describe the competition with 100 fold molar excess of unlabeled homologous self, Sp1 consensus, Mut SMP-Sp1 and nonspecific SRY oligonucleotide duplex respectively.

3 sense/Luc-SMP-XhoI antisense and Luc-SMP-3 sense/Mut Luc 3–3 antisense. The PCR amplification was performed using step cycles (94°C for 1 min, 62°C for 30 s, 72°C 30 s) for 35 cycles with a final extension at 72°C for 10 minutes. Both the PCR products were purified using QIAquick Gel Extraction Kit. DNA was eluted using 30 μl of autoclaved deionised water. 5 μl of each PCR product was used as a template for the second round of PCR. For example: for construction of mutant Sp1 site: 5μl each of the PCR product Mut Sp1 sense/Luc-SMP-XhoI antisense and Luc-5 sense/Mut Sp1 antisense was used as template. For construction of mutant Sp1 and mutant C/EBP, Luc-5 and Luc-SMP-XhoI was used as forward and reverse primers. For construction of mutant Luc 3–1, Luc 3–2 and Luc 3–3, Luc-3 and Luc-SMP-XhoI was used as forward and reverse primers. PCR amplification was carried out using the same parameters as mentioned above. Then the PCR products were purified using QIAquick Gel Extraction Kit. The fragments with mutated transcription factor binding sites, having KpnI and XhoI restriction sites and pGL3-Basic vector were digested with KpnI and XhoI enzyme. The fragments were then ligated into restriction enzyme digested pGL3-Basic vector using DNA ligase. The cloned fragments were then confirmed by vector specific PCR using RV and GL2 primer, and the mutation was confirmed by sequencing.

Transient transfection and luciferase assay

Transient transfections were carried out using RAG cells (mouse renal adenocarcinoma cell line) as SMP30 is also expressed in kidney. The cells were plated at a density of 2 × 10^5 cells per well in six well plates, 18 h before transfection. For transient transfection 2 μg of respective reporter plasmid DNA and 0.5 μg of pSV-β-gal control vector

Figure 18

Electrophoretic mobility shift assay to confirm the binding of C/EBP transcription factor. *Lane 1–5*, labeled mutated C/EBP oligonucleotide duplex with 6 μg RLNE; *Lane 2*, C/EBPβ antibody; *Lane 3–5*, describe the competition with 100 fold molar excess of unlabeled homologous self, SMP-C/EBP and C/EBP consensus. *Lane 6–11*, labeled SMP-C/EBP oligonucleotide duplex with 6 μg RLNE; *Lane 7*, C/EBPβ antibody; *Lane 8–11*, describe the competition with 100 fold molar excess of unlabeled homologous self, C/EBP consensus, Mut SMP-C/EBP and nonspecific SRY oligonucleotide duplex respectively. Antibody shift is seen with SMP-C/EBP only and not with mutated SMP-C/EBP.

(Promega, USA) or 100 ng of pRL-TK control vector were cotransfected into cells using FuGENE reagent (Roche, USA). After 24 h post transfection, the cells were harvested, lysed, centrifuged and the lysate was used for luciferase assay using the luciferase assay system (Promega, USA). The colorimetric β-galactosidase assay was performed using β-Gal assay kit (Invitrogen, USA) and luciferase activity was divided by the β-galactosidase activity to normalize for transfection efficiency. For transfection of mutated constructs Renella was used as an internal control and dual luciferase assay was preformed to measure the luciferase reading as per manufacturer's instruction

Table 5: Primers and oligonucleotide used for site- directed mutagenesis.

Mut Luc-3-1	GCTGgAGGCcTAGCTCTGTAGCAGAgTACAccCAAG
Mut Luc-3-2	CAgGGTCCTcGTTCcATtCCaG
Mut Luc-3-3	CCAGTgCAgACgAGCAAGCggCTGTATATgC
SP1-SMP	GCTCCCCCCCCCCGCCCCCCCCCAGGG
Mut-SP1	GCTCCtCCtCCtCGtCtCCCtCCAG
C/EBP-SMP	ACTGATGTACACATTCCTAAAACTGGC
Mut-C/EBP	ACTGgTGgACACAggCCTAggACTGGC

Table 6: Oligonucleotide of the three footprints between -513 to -352 bp used for EMSA.

Footprint	DNase I protected region	Transcription factor
Luc3-1	GGAGCTGGAGGCATAGCTCTGTAGCAGAATACATTCAAGGT	CdxA
Luc3-2	TTCAAGGTCCTAGTTCTATCCCAG	GATA-2
Luc3-3	AACTACCAGTACAAACAAGCAAGCAACTGTATACAT	SRY

(Promega, USA). All the transfections were repeated in duplicates in three to five independent experiments. The number of independent experiments is being mentioned in respective figure legends.

Abbreviations

SMP30: Senescence Marker Protein 30; EMSA: Electrophoretic Mobility Shift Assay; RLNE: Rat Liver Nuclear Extract.

Authors' contributions

PCS and NM conceived the idea, designed and planned the experiments. BR and PCS wrote the manuscript. BR and RSP were involved in all experimentations. PRD was involved in designing and preparation of promoter-reporter constructs. All authors have analyzed the data and agreed with the final version of the manuscript.

Acknowledgements

This research was supported by Department of Biotechnology, Govt. of India, New Delhi, India. PRD is supported by pre-doctoral research fellowship from Council of Scientific and Industrial Research (CSIR), New Delhi, India. We thank Dr. Soumen Chakraborty for his advice in preparation of site directed mutated constructs and transfection experiments.

References

1. Fujita T: **Senescence marker protein-30 (SMP30): Structure and biological function.** *Biochem Biophys Res Commun* 1999, **254**:1-4.
2. Fujita T, Shirasawa T, Maruyama N: **Isolation and characterization of genomic and cDNA clones encoding mouse senescence marker protein-30 (SMP30).** *Biochim Biophys Acta* 1996, **1308**:49-57.
3. Ishigami A, Kondo Y, Nanba R, Oshsawa T, Handa S, Kubo S, Akita M, Maruyama N: **SMP30 deficiency in mice causes an accumulation of neural lipids and phospholipids in the liver and shortens the life span.** *Biochem Biophys Res Commun* 2004, **315**:575-580.
4. Ishigami A, Fujita T, Handa S, Shirasawa T, Koseki H, Kitamura T, Enomoto N, Sato N, Shimosawa T, Maruyama N: **Senescence marker protein-30 knockout mouse liver is highly susceptible to tumor necrosis factor-alpha- and Fas-mediated apoptosis.** *Am J Pathol* 2002, **161**:1273-1281.
5. Kondo Y, Inai Y, Sato Y, Handa S, Kubo S, Shimokado K, Goto S, Nishikimi M, Maruyama N, Ishigami A: **Senescence marker protein 30 functions as gluconolactonase in L-ascorbic acid biosynthesis, and its knockout mice are prone to scurvy.** *Proc Natl Acad Sci USA* 2006, **103**:5723-5728.
6. Sar P, Rath B, Subudhi U, Chainy GB, Supakar PC: **Alterations in expression of senescence marker protein-30 gene by 3,3',5-triiodo-L: -thyronine (T(3)).** *Mol Cell Biochem* 2007, **303**:239-242.
7. Supakar PC, Fujita T, Maruyama N: **Identification of novel sequence-specific nuclear factors interacting with mouse senescence marker protein-30 gene promoter.** *Biochem Biophys Res Commun* 2002, **272**:436-440.
8. Liu Y, Michalopoulos GK, Zarnegar R: **Structural and functional characterization of the mouse hepatocyte growth factor gene promoter.** *J Biol Chem* 1994, **269**:4152-4160.
9. Mitchell PJ, Tjian R: **Transcriptional regulation in mammalian cells by sequence-specific DNA binding proteins.** *Science* 1989, **245**:371-378.
10. Yamada K, Tanaka T, Miyamoto K, Noguchi T: **Sp family members and nuclear factor-Y cooperatively stimulate transcription from the rat pyruvate kinase M gene distal promoter region via their direct interactions.** *J Biol Chem* 2000, **275**:8129-8137.
11. Lee YH, Williams SC, Baer M, Sterneck E, Gonzalez FJ, Johnson PF: **The ability of C/EBP beta but not C/EBP alpha to synergize with an Sp1 protein is specified by the leucine zipper and activation domain.** *Mol Cell Biol* 1997, **17**:2038-2047.
12. Turner ME, Martin C, Martins AS, Dunmire J, Farkas J, Ely DL, Milsted A: **Genomic and expression analysis of multiple Sry loci from a single Rattus norvegicus Y chromosome.** *BMC Genet* 2007, **8**:11.
13. Dewing P, Chiang CW, Sinchak K, Sim H, Fernagut PO, Kelly S, Chesselet MF, Micevych PE, Albrecht KH, Harley VR, Vilain E: **Direct regulation of adult brain function by the male-specific factor SRY.** *Curr Biol* 2006, **16**:415-420.
14. Dubin RA, Ostrer H: **Sry is a transcriptional activator.** *Mol Endocrinol* 1996, **8**:1182-1192.
15. Yuan X, Lu ML, Li T, Balk SP: **SRY interacts with and negatively regulates androgen receptor transcriptional activity.** *J Biol Chem* 2001, **276**:46647-46654.
16. Terzic N, Vujcic M, Ristic-Fira A, Krstic-Demonacos M, Milanovic D, Kanazir DT, Ruzdijic S: **Effects of age and dexamethasone treatment on glucocorticoid response element and activating protein-1 binding activity in rat brain.** *J Gerontol A Biol Sci Med Sci* 2003, **58**:297-303.

Myasthenia Gravis Experimentally Induced with Muscle-specific Kinase

KAZUHIRO SHIGEMOTO,[a,*] SACHIHO KUBO,[b] CHEN JIE,[c] NAOHITO HATO,[d] YASUHITO ABE,[e] NORIFUMI UEDA,[e] NAOTO KOBAYASHI,[f] KENJI KAMEDA,[g] KATSUMI MOMINOKI,[h] ATSUO MIYAZAWA,[i] AKIHITO ISHIGAMI,[b] SEIJI MATSUDA,[c] AND NAOKI MARUYAMA[b]

[a]*Department of Preventive Medicine, Ehime University School of Medicine, Ehime, Japan*

[b]*Department of Molecular Pathology, Tokyo Metropolitan Institute for Gerontology, Tokyo, Japan*

[c]*Department of Integrated Basic Medical Science, Ehime University School of Medicine, Ehime, Japan*

[d]*Department of Otolaryngology, Ehime University School of Medicine, Ehime, Japan*

[e]*Department of Molecular Pathology, Ehime University School of Medicine, Ehime, Japan*

[f]*Department of Bioscience, Medical Education Center, Ehime University School of Medicine, Ehime, Japan*

[g]*Department of Bioscience, The Integrated Center for Science, Ehime University, Ehime, Japan*

[h]*Department of Animal Resources, Advanced Science Research Center, Okayama University, Okayama, Japan*

[i]*Membrane Dynamics Project, RIKEN Harima Institute, Hyogo, Japan*

Here we present the first evidence that muscle-specific kinase (MuSK) antigen can cause myasthenia in animals. MuSK is expressed at the postsynaptic membranes of neuromuscular junctions (NMJ) and forms complexes with acetylcholine receptors (AChR) and rapsyn. MuSK is activated by agrin, which is released from motoneurons, and induces AChR clustering and subsequent formation of NMJ in embryos. Notably, autoantibodies against MuSK were found in a proportion of patients with generalized myasthenia gravis (MG) but without the characteristic AChR autoantibodies. However, MuSK autoantibodies had no known pathogenic potential, and animals immunized with purified MuSK proteins did not develop MG in former studies. In contrast, we have now injected rabbits with MuSK ectodomain protein *in vivo* and evoked a MG-like muscle weakness with a reduction of AChR clustering at the NMJ. Our results showed that MuSK is required for maintenance of synapses and that interference with that function by MuSK antibodies causes myasthenic weakness. *In vitro,* AChR clustering in myotubes is induced by agrin and agrin-independent inducers, which do not activate MuSK. Neither the receptor nor the activation mechanisms of AChR clustering induced by agrin-independent inducers has been identified with certainty, but MuSK autoantibodies in myasthenic animals inhibited both agrin and agrin-independent AChR clustering. MuSK plays multiple roles in pre-patterning of the postsynaptic membrane before innervation and formation of NMJ in embryos. Some of these mechanisms may also participate in the maintenance of mature NMJ. This model system would provide new knowledge about the molecular pathogenesis of MG and MuSK functions in mature NMJ.

Key words: myasthenia gravis (MG); experimental autoimmune MG (EAMG); muscle-specific kinase (MuSK); acetylcholine receptor (AChR); neuromuscular junction (NMJ); congenital myasthenic syndromes (CMS)

Introduction

Although autoantibodies against muscle-specific kinase (MuSK) have been found in patients with myasthenia gravis (MG),[1] any pathogenic contribution of MuSK antibodies to the muscle weakness that typifies MG has remained in dispute. That is, until now, MuSK

Present address: Tokyo Metropolitan Institute of Gerontology, Research Team for Molecular Biomarkers, Tokyo, Japan.

Address for correspondence: Kazuhiro Shigemoto, Tokyo Metropolitan Institute of Gerontology, Research Team for Molecular Biomarkers, Sakaecho 35-2, Itabashi-Ku, Tokyo 173-0015, Japan. Voice: +81-3-3964-3241, ext. 3025; fax: +81-3-3579-4776.

kazshige@tmig.or.jp

Ann. N.Y. Acad. Sci. 1132: 93–98 (2008).
doi: 10.1196/annals.1405.002

antibodies have not produced experimental autoimmune MG (EAMG).[2,3] Here we describe the recent progress toward understanding this phenomenon.

Autoantibodies against MuSK

About 80% of patients with MG have autoantibodies against acetylcholine receptor (AChR). A seminal experiment by Patrick and Lindstrom demonstrated the pathogenicity of autoantibodies to AChR about 30 years ago.[4] Although a number of studies have documented that AChR antibodies cause structural and functional damage to the neuromuscular junction (NMJ), autoantigens, in the nearly 20% of MG patients without such antibodies, remained obscure.[1] Then, in 2001, Hoch *et al.* identified antibodies against MuSK in a proportion of patients with generalized MG.[1] MuSK is required for clustering of AChR during the formation of NMJ and is expressed predominantly at the postsynaptic membrane in mature NMJ.[5,6] In MuSK knockout mice, AChRs fail to cluster opposite to growing motoneuron terminals on the surfaces of myotubes.[7] Additionally, a case of heteroalleric MuSK mutations that caused the reduction of MuSK expression has been associated with congenital myasthenic syndrome (CMS).[8] Further, the reduction of MuSK expression in rat muscles *in vivo* upon RNA interference induced disassembly of synapses.[9] Even though the function of MuSK in mature NMJ is still uncertain, a causal relationship between MuSK autoantibodies and MG has been proposed.[1,10,11]

Recent studies by Vincent and others showed that the frequency of MuSK antibodies in MG patients who were AChR seronegative (lacked autoantibodies to AChR) varied from 4 to 50%.[11–17] We detected MuSK antibodies in 29% of seronegative MG patients but not in any MG patients with AChR antibodies (seropositive MG) or with other autoimmune diseases.[16] Previously, we identified antibodies against a recombinant MuSK fusion protein with human alkaline phosphatase (AP) in seropositive MG patients[15] and later revealed that 8.8% of seropositive MG patients had autoantibodies to AP but not to MuSK.[16] We are currently studying the clinical significance of the autoantibodies to AP in seropositive MG.

Clinical features of patients with MG and MuSK antibodies are distinctive. Such patients often have severe bulbar dysfunctions that can be difficult to treat effectively with immunosuppressive and immunomodulatory strategies, and atrophy of facial and tongue muscles is common.[12,13,18,19] After the identification of MuSK antibodies in MG patients, laboratory quantification of these antibodies is now required to confirm the diagnosis of MG, the appropriate clinical treatment, as well as the presence of AChR antibodies.[18,20,21]

Experimental Autoimmune MG

Although MuSK antibodies are present in some seronegative MG patients and the clinical features are distinctive, proving the pathogenicity of MuSK antibodies has been difficult because these antibodies did not induce myasthenia in experimental animals. Formerly, the pathogenicity of AChR antibodies was shown when rabbits injected with AChR protein purified from electric eels developed muscle weakness and paralysis.[4] Injection of eel AChR protein stimulates the production of antibodies that cross-react with rabbit AChR at the NMJ. Electrophysiological studies confirmed that the flaccid paralysis in this animal model resembled that in MG patients. Similarly, EAMG appeared in other species after immunization with purified AChR protein. In addition, the antibodies to AChR in human MG patients could passively transfer disease to mice.[22] Therefore, creating an EAMG model induced by MuSK antibodies was indispensible for proving the pathogenicity of MuSK antibodies and investigating their pathogenic mechanisms in MG.[10,20,21]

To pursue this objective, we recently immunized rabbits with MuSK ectodomain, which caused myasthenic weakness and produced electromyographic findings that were compatible with a diagnosis of MG, as shown by Patrick and Lindstrom.[23] The extracellular segment of MuSK comprises five distinct domains, i.e., four immunoglobulin-like domains and one cysteine-rich region.[5,6] The fusion protein expression constructs we generated consisted of mouse MuSK ectodomain with the Fc region of human IgG1 or His-tag and were used to transfect COS-7 cells.[23] The recombinant MuSK-Fc and MuSK-His proteins secreted were purified by using protein-A Sepharose and histidine affinity columns, respectively (FIG. 1). New Zealand white rabbits were then immunized with 100–400 mg of this purified MuSK recombinant protein. After three to four injections of MuSK protein, all six treated rabbits manifested flaccid paralysis (FIG. 2). Sera from the paretic rabbits contained high titers of MuSK antibodies that reacted specifically with MuSK molecules as observed by testing sera from MG patients with MuSK antibodies.[1,24] The paretic rabbits developed severe muscular exhaustion revealed by histological studies showing alterations in muscle fibers

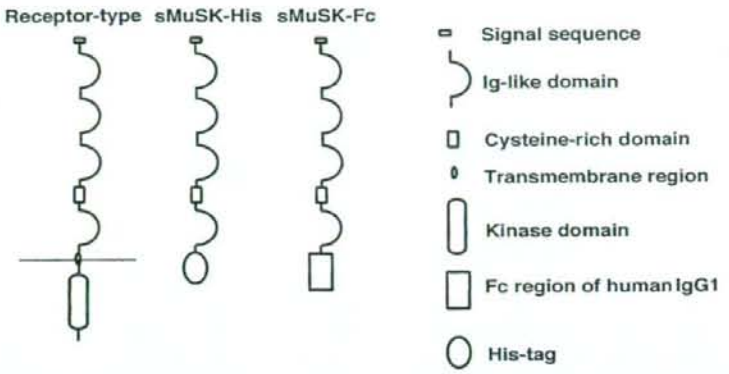

FIGURE 1. Schematic representation of the muscle-specific kinase (MuSK) domain structure and expression of secretory MuSK proteins in COS-7 cells. The domain structures of recombinant secretory MuSK protein (MuSK-His and MuSK-Fc) and receptor-type MuSK are shown. The whole coding region of the MuSK extracellular domain was fused with the His-tag or Fc region of human IgG1 as shown.

ranging from subtle to angular atrophy intermingled with normal muscle. Atrophic changes of this type can result from MG, reduced mechanical activity of muscles, or cachexia. Repetitive electromyograms of a paretic rabbit were then done to measure the result of stimulating the retroauricular branch at 20 Hz and recording responses from the retroauricular muscle. The compound muscle action potential (CMAP) showed a decremental pattern, consistent with MG.[23] However, the injection of ACh esterase inhibitor did not significantly offset the CMAP decrement or decrease the symptoms. Importantly, the induction of EAMG by MuSK antibodies is not limited to rabbits, i.e., we and others have also produced EAMG in mice by injecting MuSK protein (FIG. 2).[25]

AChR Clustering and Structure of NMJ in Rabbits with EAMG and MuSK Antibodies

The clustering of AChR necessary for NMJ formation is completely abolished in MuSK knockout mice,[7] and AChR clustering at the NMJ is reduced in subjects with CMS and MuSK mutations.[8] In a previous RNA interference experiment, injection of double-stranded RNA (dsRNA) targeting MuSK diminishes the expression of MuSK protein and AChR clusters in rat muscle fibers *in vivo*, whereas dsRNA targeting nonessential proteins does not have any effect (RNA-interference experiment).[9] Therefore, we examined the expression of AChR at NMJ in soleus muscles of paretic and normal rabbits by fluorescence microscopy after applying a rhodamine-conjugated AChR agonist, a-bungarotoxin. Images of AChR clustering were then recorded by using a digital camera.[23] The sizes and optical densities were measured using National Institute of Health (NIH) image analysis software with unprocessed digitized NIH images (version 1-62; http://rsb.info.nih.gov/nih-image). The results unequivocally pictured a significantly reduced area and intensity of AChR fluorescence in the paretic rabbits compared with their normal counterparts. In addition, a structural examination showed that the size and branching of the NMJ were significantly diminished in paretic rabbits. Similar changes of NMJ structure were observed in rats with reduced expression of MuSK evident by RNA interference,[9] in a patient with CMS and MuSK mutations, and in mice expressing the missense mutation by electroporation experiments.[8] Our results demonstrated that MuSK antibodies also elicited synaptic changes in EAMG, including the reduced expression of surface AChR at postsynaptic membranes of NMJ. Further examination of MuSK knockout mice disclosed presynaptic defects in addition to postsynaptic ones,[7] indicating that MuSK is also required for presently unidentified retrograde signals to maintain the presynaptic structure in mature NMJ.

Pathogenic Mechanisms of MuSK Antibodies in AChR Clustering at NMJ

MuSK plays multiple roles in clustering AChR during development of the postsynaptic membrane of NMJ. Contact of the motor-nerve growth cone with

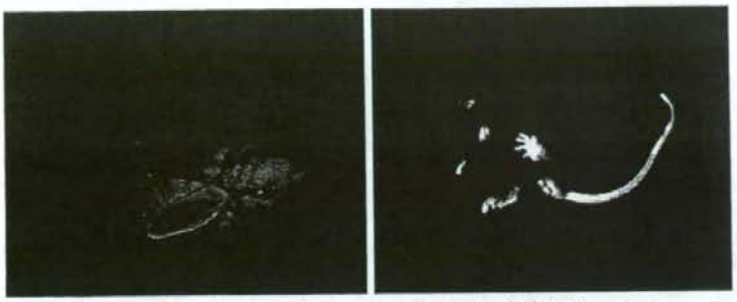

FIGURE 2. Manifestation of muscle weakness after injection of purified MuSK proteins in experimental animals (*left*, a paretic rabbit; *right*, a paretic mouse).

the muscle induces a narrow, distinct, endplate zone in the mid-muscle that is marked by a high density of AChR clustering.[26–29] In this step, agrin released from motoneurons activates MuSK and redistributes AChR clusters to synaptic sites. However, a direct physical interaction between MuSK and agrin has so far not been demonstrated, despite many efforts to do so.[27] Thus, the mechanisms of MuSK activation and the following events remain obscure, although a co-receptor of MuSK, co-ligand of agrin or either post-translational modification of agrin or MuSK have been postulated. Intriguingly, MuSK is also required for organizing a primary synaptic scaffold to establish the post-synaptic membrane.[30,31] Preceding muscle innervations, AChR clusters form at the central regions of muscle fibers, creating an endplate zone that is somewhat broader than that in innervated muscle. Thus, MuSK is required for pre-patterning of AChR clustering in the absence of motor innervation. The scenario of MuSK's roles in the process is somewhat complicated; possibly an element other than agrin achieves activation of MuSK and triggers postsynaptic specialization at the NMJ, and/or MuSK acts as a primary scaffold molecule without activation. The listed pleiotropic roles of MuSK in AChR clustering at NMJ development could also require the maintenance of mature NMJ. Studies performed *in vivo* have shown that synaptic AChRs intermingle completely over a period of approximately 4 days and that many extrasynaptic AChRs are incorporated into the synapse at the mature NMJ, although the synaptic membrane in adult muscle appears to be macroscopically stable.[32,33] Therefore, the mechanisms at play in AChR clustering during NMJ development are also required in mature NMJ when postsynaptic complexes, including AChR and MuSK, are dynamically turning over for maintenance.

To elucidate the mechanisms of AChR clustering at NMJ, a number of studies were performed using cultured C2C12 myotubes. Agrin induces clustering of AChR in C2C12 myotubes following MuSK autophosphorylation.[26,27,29] This event *in vitro* represents a major cascade of AChR clustering at the NMJ after innervation by motoneurons.[27,34–36] Laminin-1 and the *N*-acetylgalactosamine (GalNAc)-specific lectin *Vicia villosa* agglutinin (VVA-B4) can induce AChR clustering in C2C12 myotubes without activation of MuSK.[34,37–40] Neither the receptor nor the activation mechanisms of AChR clustering induced by agrin-independent inducers has been identified with certainty. However, these mechanisms may also play important roles in the maintenance of NMJs via agrin-independent pathways and in their formation, as shown by genetic studies.[30,31]

In their previous study, Hoch *et al.* observed that the MuSK antibodies of MG patients inhibited agrin-induced AChR clustering in C2C12 myotubes.[1] We also found that agrin-induced clustering of AChR was strongly blocked in the presence of MuSK antibodies, whereas absorption of the antibodies with purified MuSK products prevented this blocking effect.[23] Thus, MuSK antibodies were responsible for inhibiting the formation of agrin-induced AChR clustering. We also perceived that MuSK-specific antibodies strongly inhibited AChR clustering induced by all known agrin-independent pathways as well as by agrin itself.

Conclusions

In our experimental model of myasthenia, MuSK antibodies routinely mediated pathogenesis in rabbits and mice.[23,25] Consequently, we now believe that MuSK antibodies cause MG in patients. However,

the pathogenic mechanisms of these antibodies entail multiple events in which MuSK acts as a multifunctional platform from which to regulate synapse formation and maintenance. These are reflected in a diversity of clinical features ranging from typical MG to a multitude of variants.[12,13,18,19]

AChR antibodies have been shown to affect neuromuscular transmission by three main mechanisms: (a) binding and activation of complement at the NMJ; (b) accelerated degradation of AChR molecules cross-linked by antibodies (antigenic modulation); and (c) functional AChR block.[20,21] Intriguingly, MuSK antibodies in MG patients are mainly of the IgG4 subclass, which does not activate complement.[41] Electron microscopic observations of NMJ in the EAMG rabbits demonstrated a significant reduction of synaptic folds but no destruction, thus our EAMG model resembles the phenotypes of MG with MuSK antibodies. MuSK antibodies against compound antigenic determinants on the extracellular domain may elicit pathogenic effects through antigenic modulation and/or restraint of MuSK functions,[41] and the consequences of these effects range from a partial to entire loss of MuSK functions.

Recently, a new MuSK-interacting cytoplasmic protein, called Dok-7, has been discovered.[42] Dok-7 knockout mice underwent a marked disruption of neuromuscular synaptogenesis that was indistinguishable from the features found in MuSK-deficient mice. Mutations in Dok-7 caused a genetic form of limb-girdle myasthenia (CMS).[43,44] Some clinical features of these patients resemble the severe type of MG with MuSK antibodies[44]; therefore, the EAMG model with MuSK antibodies presented here promises to facilitate resolution of the pathogenic basis of MG and CMS at the molecular level and identification of beneficial treatment strategies against them.

Acknowledgments

We thank Ms. P. Minick for excellent editorial assistance. This study was supported by a Health Science Research Grant, Research on Psychiatric and Neurological Diseases and Mental Health, from the Ministry of Health, Labor, and Welfare, Japan; and by a grant-in-aid for Scientific Research from the Ministry of Education, Science, and Culture, Japan; and by a grant from the Kato Memorial Trust for Nambyo Research, Japan; and by a grants from Kurozumi Medical Foundation, Japan. We are also grateful to the staff of the Integrated Center for Science of Ehime University for assistance with animal care and sequence analysis.

Conflicts of Interest

The authors declare no conflicts of interest.

References

1. Hoch, W., J. McConville, S. Helms, *et al.* 2001. Autoantibodies to the receptor tyrosine kinase MuSK in patients with myasthenia gravis without acetylcholine receptor antibodies. Nat. Med. **7:** 365–368.
2. Lindstrom, J. 2004. Is "seronegative" MG explained by autoantibodies to MuSK? Neurology **62:** 1920–1921.
3. Selcen, D., T. Fukuda, X.M. Shen & A.G. Engel. 2004. Are MuSK antibodies the primary cause of myasthenic symptoms? Neurology **62:** 1945–1950.
4. Patrick, J. & J. Lindstrom. 1973. Autoimmune response to acetylcholine receptor. Science **180:** 871–872.
5. Ganju, P., E. Walls, J. Brennan & A.D. Reith. 1995. Cloning and developmental expression of Nsk2, a novel receptor tyrosine kinase implicated in skeletal myogenesis. Oncogene **11:** 281–290.
6. Valenzuela, D.M., T.N. Stitt, P.S. DiStefano, *et al.* 1995. Receptor tyrosine kinase specific for the skeletal muscle lineage: expression in embryonic muscle, at the neuromuscular junction, and after injury. Neuron **15:** 573–584.
7. DeChiara, T.M., D.C. Bowen, D.M. Valenzuela, *et al.* 1996. The receptor tyrosine kinase MuSK is required for neuromuscular junction formation in vivo. Cell **85:** 501–512.
8. Chevessier, F., B. Faraut, A. Ravel-Chapuis, *et al.* 2004. MUSK, a new target for mutations causing congenital myasthenic syndrome. Hum. Mol. Genet. **13:** 3229–3240.
9. Kong, X.C., P. Barzaghi & M.A. Ruegg. 2004. Inhibition of synapse assembly in mammalian muscle in vivo by RNA interference. EMBO Rep. **5:** 183–188.
10. Vincent, A. 2002. Unravelling the pathogenesis of myasthenia gravis. Nat. Rev. Immunol. **2:** 797–804.
11. Vincent, A., J. Bowen, J. Newsom-Davis & J. McConville. 2003. Seronegative generalised myasthenia gravis: clinical features, antibodies, and their targets. Lancet Neurol. **2:** 99–106.
12. Evoli, A., P.A. Tonali, L. Padua, *et al.* 2003. Clinical correlates with anti-MuSK antibodies in generalized seronegative myasthenia gravis. Brain **126:** 2304–2311.
13. Sanders, D.B., K. El-Salem, J.M. Massey, *et al.* 2003. Clinical aspects of MuSK antibody positive seronegative MG. Neurology **60:** 1978–1980.
14. Yeh, J.H., W.H. Chen, H.C. Chiu & A. Vincent. 2004. Low frequency of MuSK antibody in generalized seronegative myasthenia gravis among Chinese. Neurology **62:** 2131–2132.
15. Ohta, K., K. Shigemoto, S. Kubo, *et al.* 2004. MuSK antibodies in AChR Ab-seropositive MG vs AChR Ab-seronegative MG. Neurology **62:** 2132–2133.
16. Ohta, K., K. Shigemoto, S. Kubo, *et al.* 2005. MuSK Ab described in seropositive MG sera found to be Ab to alkaline phosphatase. Neurology **65:** 1988.
17. Vincent, A., J. McConville, M.E. Farrugia, *et al.* 2003. Antibodies in myasthenia gravis and related disorders. Ann. N.Y. Acad. Sci. **998:** 324–335.

18. Bartoccioni, E., F. Scuderi, G.M. Minicuci, *et al.* 2006. Anti-MuSK antibodies: correlation with myasthenia gravis severity. Neurology **67:** 505–507.
19. Deymeer, F., O. Gungor-Tuncer, V. Yilmaz, *et al.* 2007. Clinical comparison of anti-MuSK- vs anti-AChR-positive and seronegative myasthenia gravis. Neurology **68:** 609–611.
20. Conti-Fine, B.M., M. Milani & H.J. Kaminski. 2006. Myasthenia gravis: past, present, and future. J. Clin. Invest. **116:** 2843–2854.
21. Vincent, A., B. Lang & K.A. Kleopa. 2006. Autoimmune channelopathies and related neurological disorders. Neuron **52:** 123–138.
22. Toyka, K.V., D.B. Drachman, D.E. Griffin, *et al.* 1977. Myasthenia gravis. Study of humoral immune mechanisms by passive transfer to mice. N. Engl. J. Med. **296:** 125–131.
23. Shigemoto, K., S. Kubo, N. Maruyama, *et al.* 2006. Induction of myasthenia by immunization against muscle-specific kinase. J. Clin. Invest. **116:** 1016–1024.
24. Scuderi, F., M. Marino, L. Colonna, *et al.* 2002. Anti-p110 autoantibodies identify a subtype of "seronegative" myasthenia gravis with prominent oculobulbar involvement. Lab. Invest. **82:** 1139–1146.
25. Jha, S., K. Xu, T. Maruta, M. Oshima, *et al.* 2006. Myasthenia gravis induced in mice by immunization with the recombinant extracellular domain of rat muscle-specific kinase (MuSK). J. Neuroimmunol. **175:** 107–117.
26. Ruegg, M.A., K.W. Tsim, S.E. Horton, *et al.* 1992. The agrin gene codes for a family of basal lamina proteins that differ in function and distribution. Neuron **8:** 691–699.
27. Glass, D.J., D.C. Bowen, T.N. Stitt, *et al.* 1996. Agrin acts via a MuSK receptor complex. Cell **85:** 513–523.
28. Cohen, I., M. Rimer, T. Lomo & U.J. McMahan. 1997. Agrin-induced postsynaptic-like apparatus in skeletal muscle fibers in vivo. Mol. Cell Neurosci. **9:** 237–253.
29. Ferns, M., M. Deiner & Z. Hall. 1996. Agrin-induced acetylcholine receptor clustering in mammalian muscle requires tyrosine phosphorylation. J. Cell. Biol. **132:** 937–944.
30. Lin, W., R.W. Burgess, B. Dominguez, *et al.* 2001. Distinct roles of nerve and muscle in postsynaptic differentiation of the neuromuscular synapse. Nature **410:** 1057–1064.
31. Yang, X., S. Arber, C. William, *et al.* 2001. Patterning of muscle acetylcholine receptor gene expression in the absence of motor innervation. Neuron **30:** 399–410.
32. Akaaboune, M., S.M. Culican, S.G. Turney & J.W. Lichtman. 1999. Rapid and reversible effects of activity on acetylcholine receptor density at the neuromuscular junction in vivo. Science **286:** 503–507.
33. Akaaboune, M., R.M. Grady, S. Turney, *et al.* 2002. Neurotransmitter receptor dynamics studied in vivo by reversible photo-unbinding of fluorescent ligands. Neuron **34:** 865–876.
34. Gautam, M., T.M. DeChiara, D.J. Glass, *et al.* 1999. Distinct phenotypes of mutant mice lacking agrin, MuSK, or rapsyn. Brain Res. Dev. Brain Res. **114:** 171–178.
35. Burgess, R.W., Q.T. Nguyen, Y.J. Son, *et al.* 1999. Alternatively spliced isoforms of nerve- and muscle-derived agrin: their roles at the neuromuscular junction. Neuron **23:** 33–44.
36. Gautam, M., P.G. Noakes, L. Moscoso, *et al.* 1996. Defective neuromuscular synaptogenesis in agrin-deficient mutant mice. Cell **85:** 525–535.
37. Sanes, J.R. & J.M. Cheney. 1982. Lectin binding reveals a synapse-specific carbohydrate in skeletal muscle. Nature **300:** 646–647.
38. Sugiyama, J.E., D.J. Glass, G.D. Yancopoulos & Z.W. Hall. 1997. Laminin-induced acetylcholine receptor clustering: an alternative pathway. J. Cell. Biol. **139:** 181–191.
39. Martin, P.T. & J.R. Sanes. 1995. Role for a synapse-specific carbohydrate in agrin-induced clustering of acetylcholine receptors. Neuron **14:** 743–754.
40. Marangi, P.A., S.T. Wieland & C. Fuhrer. 2002. Laminin-1 redistributes postsynaptic proteins and requires rapsyn, tyrosine phosphorylation, and Src and Fyn to stably cluster acetylcholine receptors. J. Cell. Biol. **157:** 883–895.
41. McConville, J., M.E. Farrugia, D. Beeson, *et al.* 2004. Detection and characterization of MuSK antibodies in seronegative myasthenia gravis. Ann. Neurol. **55:** 580–584.
42. Okada, K., A. Inoue, M. Okada, *et al.* 2006. The muscle protein Dok-7 is essential for neuromuscular synaptogenesis. Science **312:** 1802–1805.
43. Beeson, D., O. Higuchi, J. Palace, *et al.* 2006. Dok-7 mutations underlie a neuromuscular junction synaptopathy. Science **313:** 1975–1978.
44. Palace, J., D. Lashley, J. Newsom-Davis, *et al.* 2007. Clinical features of the DOK7 neuromuscular junction synaptopathy. Brain **130:** 1507–1515.

The American Journal of Pathology, Vol. 173, No. 4, October 2008

DOI: 10.2353/ajpath.2008.080388

Neurobiology

Accumulation of Citrullinated Proteins by Up-Regulated Peptidylarginine Deiminase 2 in Brains of Scrapie-Infected Mice

A Possible Role in Pathogenesis

Byungki Jang,*† Eunah Kim,* Jin-Kyu Choi,* Jae-Kwang Jin,* Jae-Il Kim,‡ Akihito Ishigami,§ Naoki Maruyama,§ Richard I. Carp,‡ Yong-Sun Kim,*† and Eun-Kyoung Choi*

From the Ilsong Institute of Life Science, Hallym University, Anyang, Republic of Korea; the Department of Microbiology,† College of Medicine, Hallym University, Chuncheon, Republic of Korea; the New York State Institute for Basic Research in Developmental Disabilities,‡ Staten Island, New York; and the Aging Regulation,§ Tokyo Metropolitan Institute of Gerontology, Tokyo, Japan*

Peptidylarginine deiminases (PADs), which are a group of posttranslational modification enzymes, are involved in protein citrullination (deimination) by the conversion of peptidylarginine to peptidylcitrulline in a calcium concentration-dependent manner. Among the PADs, PAD2 is widely distributed in various tissues and is the only type that is expressed in brain. To elucidate the involvement of protein citrullination by PAD2 in the pathogenesis of brain-specific prion diseases, we examined the profiles of citrullinated proteins using the brains of scrapie-infected mice as a prion disease model. We found that, compared with controls, increased levels of citrullinated proteins of various molecular weights were detected in different brain sections of scrapie-infected mice. In support of this data, expression levels of PAD2 protein as well as its enzyme activity were significantly increased in brain sections of scrapie-infected mice, including hippocampus, brain stem, and striatum. Additionally, the expression levels of PAD2 mRNA were increased during scrapie infection. Moreover, PAD2 immunoreactivity was increased in scrapie-infected brains, with staining detected primarily in reactive astrocytes. Using two-dimensional electrophoresis and matrix-assisted laser desorption/ionization-time of flight mass spectrometry, various citrullinated proteins were identified in the brains of scrapie-infected mice, including glial fibrillary acidic protein, myelin basic protein, enolases, and aldolases. This study suggests that accumulated citrullinated proteins and abnormal activation of PAD2 may function in the pathogenesis of prion diseases and serve as potential therapeutic targets. *(Am J Pathol 2008, 173:1131–1144; DOI: 10.2353/ajpath.2008.080388)*

Accumulation of misfolded proteins, posttranslational modification of proteins, alteration of free ion distribution, and perturbation of cellular redox homeostasis are general features of progressive neurodegenerative disorders. These changes have been observed consistently as part of the neuropathogenesis and neuropathology of prion diseases. Prion diseases are characterized by various neurological symptoms and common histopathological features such as spongiform degeneration of the central nervous system, reactive gliosis, neuronal loss, and, in some cases, formation of amyloid plaques.[1] It has been reported that all prion diseases are associated with the aberrant metabolism of prion protein (PrP). Conversion of the cellular prion protein (PrP^{C}) into an abnormal, protease-resistant and infectious isoform (PrP^{Sc}) is believed to be a principal molecular basis of prion diseases,[2] and the accumulation of PrP^{Sc} in the central nervous system is thought to be responsible for neuronal loss and/or astrocytosis.[3] In general, the pathogenic mech-

Supported by the Korea Research Foundation grant funded by Korean Government (MOEHRD, Basic Research Promotion Fund) (KRF-2006-331-E00287).

B.J. and E.K. contributed equally to this article.

Accepted for publication July 3, 2008.

Address reprint requests to Professor Eun-Kyoung Choi, Laboratory of Cellular Aging and Neurodegeneration, Ilsong Institute of Life Science, Hallym University, Anyang, Gyeonggi-do 431-060, Republic of Korea. E-mail: ekchoi@hallym.ac.kr.

anisms of neurodegenerative disorders are not fully delineated; prion diseases are no exception to this uncertainty.

Alteration of intracellular calcium (Ca^{2+}) distribution and Ca^{2+}-related proteins have a critical role in synaptic dysfunction and neuronal cell death in neurodegenerative diseases. In cultured cells, prion infection induced abnormalities in Ca^{2+} homeostasis by altering receptor-mediated intracellular Ca^{2+} responses,[4,5] suggesting a possible role of Ca^{2+} in the neuronal cell death seen in prion diseases. Peptidylarginine deiminases (PADs) are known to be directly affected by Ca^{2+} homeostasis and convert peptidylarginine to peptidylcitrulline (protein citrullination or deimination) in a Ca^{2+} concentration-dependent manner.[6,7] This modification of proteins decreases their positive charge resulting in changing the functions of native proteins.[8] PADs are found as five different isoforms in various mammalian tissues such as brain, spinal cord, spleen, and skeletal muscle.[9] Among them, only PAD type II (PAD2) is expressed in adult rat brains and its cellular localization was found in glial cells.[10–12] In a very recent report, PAD2 expression was detected in cultured Schwann cells.[13] Previous reports indicate that PAD2 is involved in the citrullination of various cerebral proteins under neurodegenerative conditions.[14] Recently, it has been reported that the abnormal accumulation of citrullinated proteins including glial fibrillary acidic protein (GFAP) and vimentin were found in Alzheimer's disease (AD)-afflicted hippocampus; increased expression of PAD2 and its enzyme activity were detected during neurodegenerative changes and were accompanied by impairment of intracellular Ca^{2+} homeostasis.[15] In multiple sclerosis (MS) patients, previous studies have revealed that citrullinated myelin basic protein (MBP) was increased to 45% of total MBP compared to healthy adults[16] and has been implicated in the pathological mechanism of MS.[17] Therefore, PAD and citrullinated proteins can be used as important factors for the diagnosis of various human diseases.[7]

To our knowledge, there are no data available regarding citrullination by PAD2 in prion diseases. Here we report for the first time that increased citrullinated proteins including GFAP, MBP, and several newly identified proteins were found in the brains of scrapie-infected mice along with increased expression of PAD2 protein and its enzyme activity. These findings suggest a possible role of citrullination in the induction of pathological changes in the brains of scrapie-infected mice.

Materials and Methods

Animals and Scrapie Strain

C57BL/6J mice, 4 to 6 weeks of age, were obtained from the Experimental Animal Center of Hallym University. The original stock of ME7 scrapie strain was kindly provided by Dr. Alan Dickinson of Agriculture and Food Research Council and Medical Research Council Institute (Edinburgh, UK): this scrapie strain was maintained by serial intracerebral passage of brain homogenate from terminally affected mice. Mice were inoculated intracerebrally with 30 μl of 1% (w/v) brain homogenate in 0.01 mol/L phosphate-buffered saline (PBS) prepared from ME7-injected C57BL mice or from control mice that had been injected with normal brain homogenate. The mice were then sacrificed under 16.5% urethane at 150 ± 10 days after inoculation with ME7 scrapie strain, a time when clinical manifestations of disease were evident. To perform a time course study, brains were also collected at different time points (50, 100, and 150 days after inoculation). Mice inoculated with normal brain homogenate remained healthy throughout the same period. For immunohistochemistry, mice were perfused transcardially with PBS followed by 4% paraformaldehyde in PBS (pH 7.4). The brains were removed immediately, postfixed in the same fixative for 2 hours at room temperature, rinsed with PBS, dehydrated with ethanol, and embedded in paraffin.

Western Blot Analysis

Brains from control and scrapie-infected mice were homogenized in modified RIPA buffer containing 50 mmol/L Tris-HCl, pH 7.4, 150 mmol/L NaCl, 2 mmol/L ethylenediaminetetraacetic acid, 1% Triton X-100, 1% Nonidet P-40, 0.25% sodium deoxycholate, and protease inhibitors.[18] The homogenates were rocked at 4°C for 1 hour and centrifuged at 18,000 × g at 4°C for 10 minutes to remove cell debris. The supernatant was collected and protein concentration was determined with a BCA protein assay kit (Pierce, Rockford, IL). Citrullinated proteins were detected by Western blot analysis as described previously.[19] Briefly, equal amounts of protein (50 μg/lane) were subjected to 12% sodium dodecyl sulfate-polyacrylamide gel electrophoresis and transferred to polyvinylidene difluoride membrane using an electrotransfer system (Bio-Rad, Hercules, CA). For detection of citrullinated proteins, citrulline residues on the polyvinylidene difluoride membrane were chemically modified by overnight incubation at 37°C in modification reagent [1 vol of 1% diacetyl monoxime/0.5% antipyrine/1 N acetic acid, and 2 vol of a mixture of 85% H_3PO_4/98% H_2SO_4/H_2O (20/25/55) containing 0.025% $FeCl_3$].[20] The membrane was then blocked with 5% nonfat dry milk in PBST (8 mmol/L Na_2HPO_4, 2 mmol/L KH_2PO_4, 138 mmol/L NaCl, 2.7 mmol/L KCl, pH 7.4, 0.05% Tween 20) for 2 hours at room temperature, then probed with an anti-modified citrulline antibody at 1:1000 (Upstate, Lake Placid, NY) in PBST overnight at 4°C. For the detection of other target proteins, the transferred polyvinylidene difluoride membranes were directly probed with either monoclonal anti-PAD2 antibody (1:2000), mouse monoclonal anti-neuron-specific enolase (1:2000) (Ab-Frontier, Seoul, Republic of Korea), rabbit polyclonal anti-aldolase C (1:1000) (Santa Cruz Biotechnology, Santa Cruz, CA), mouse monoclonal anti-MBP (1:3000) (Abcam, Cambridge, MA), or mouse monoclonal anti-β actin (1:10,000) (Sigma, St. Louis, MO) in 5% nonfat dry milk in PBST. These membranes were then incu-

bated with the appropriate secondary antibody-conjugated to horseradish peroxidase. Bound antibodies were visualized by chemiluminescent substrate as described by the manufacturer (Amersham Biosciences, Piscataway, NJ).

Reverse Transcription-Polymerase Chain Reaction (RT-PCR)

Total RNA was extracted from brain samples of control and scrapie-infected mice using TRI-reagent (Sigma) according to the manufacturer's protocols. Complementary DNA (cDNA) was generated using the Moloney murine leukemia virus reverse transcriptase (Promega, Madison, WI) according to the instructions of the manufacturer. RT-PCR was performed using primers specific for the PAD2 (665 bp; forward, 5′-CTGCGGTCTCTGGGTCCTTCCTGTA-3′ and reverse, 5′-GACCAGGCGAGAGAACAGAAATAGC-3′) and β-actin (196 bp; forward, 5′-TGTGATGGACTCCGGTGACGG-3′ and reverse, 5′- ACA GCTTCTCTTTGATGTCACGC-3′) genes. The PCR products were separated by electrophoresis on a 1% agarose gel and visualized under UV light.

Measurement of PAD2 Activity

The PAD2 activity was determined as described previously.[9] Briefly, the reaction mixture containing 100 mmol/L Tris-HCl, pH 7.5, 10 mmol/L $CaCl_2$, 5 mmol/L dithiothreitol, with or without 10 mmol/L benzoyl-L-arginine ethyl ester (Sigma), and 0.5 mg of brain protein in a final volume of 120 μl was incubated at 50°C for 1 hour. After incubation, the reaction was stopped by adding final 1 mol/L perchloric acid. Samples were cooled down on ice for 20 minutes and then centrifuged at 18,000 × *g* for 5 minutes at room temperature. Aliquots of 120 μl of supernatant were mixed with 380 μl of dH_2O and 500 μl of color developing reagent and incubated at 95°C for 15 minutes. The samples were cooled to room temperature and then the absorbance was measured at 540 nm by enzyme-linked immunosorbent assay reader (VersaMax; Molecular Devices, Sunnyvale, CA). Quantification of citrulline was determined by comparison with appropriate standards. One unit of the enzyme is defined as the amount of enzyme that deiminates 1 μmol/L of the substrate (benzoyl-L-arginine ethyl ester) in 1 minute at 50°C.

Immunohistochemistry and Double-Immunofluorescence Staining

Immunohistochemical procedures were performed using the ABC kit (Vector, Burlingame, CA) by a modification of the avidin-biotin-peroxidase method. Briefly, 6-μm sections of brain were deparaffinized with xylene and hydrated in a graded ethanol series, and then treated with 0.3% hydrogen peroxide in methyl alcohol for 20 minutes to block endogenous peroxidase. The sections were exposed to normal donkey serum (Jackson ImmunoResearch, West Grove, PA), and then incubated with mouse monoclonal antibody for PAD2 (1:500) overnight at 4°C. After washing, the sections were treated sequentially with biotinylated anti-mouse IgG and avidin-biotin-peroxidase complex, developed with diaminobenzidine-hydrogen peroxide solution (0.003% 3,3-diaminobenzidine and 0.03% hydrogen peroxide in 50 mmol/L Tris buffer), and finally counterstained with hematoxylin. For staining of citrullinated proteins, the sections were incubated in modification reagent for 2 hours at 37°C before initiation of the immunohistochemistry protocol. After three washes in PBS buffer, the sections were exposed to 10% normal donkey serum for 1 hour at room temperature and then rabbit polyclonal antibody to modified citrulline (1:4000) for 1 hour at 37°C. The subsequent procedures were performed as described above for PAD2 staining. For double-immunofluorescence staining, the sections were incubated in the following order: 10% normal donkey serum in PBS for 1 hour, rabbit polyclonal anti-PAD2 (1:100)[21] overnight at 4°C, lissamine rhodamine sulfonyl chloride (LRSC)-conjugated donkey anti-rabbit IgG (1:200) (Jackson ImmunoResearch) for 1 hour at room temperature, washed, and blocked with 10% normal goat serum in PBS for 1 hour at room temperature and then incubated with various primary antibodies as follows: mouse monoclonal anti-GFAP antisera (1:400; DAKO, Copenhagen, Denmark), mouse monoclonal anti-NeuN (1:50) (Chemicon, Temecula, CA), mouse monoclonal anti-MBP (1:3000) overnight at 4°C and finally washed and incubated with fluorescein isothiocyanate-conjugated goat anti-mouse IgG (1:200) (Jackson ImmunoResearch). For microglia staining, the lectin *Griffonia simplicifolia* (GSA) was optimized by incubating the sections in 0.5 mg/ml of trypsin in 0.05 mol/L Tris-buffered saline containing 1 mmol/L $CaCl_2$ (pH 7.6) for 5 minutes at 37°C. Biotinylated lectin GSA B4-isolectin (Sigma) was then added for 1 hour at room temperature, followed by fluorescein isothiocyanate-labeled streptavidin (Zymed, San Francisco, CA). The sections were examined with a LSM 510 confocal laser-scanning microscope (Carl Zeiss, Oberkochen, Germany).

Two-Dimensional Gel Electrophoresis (2-DE) and Proteome Analysis

Protein extraction and 2-DE were performed as reported previously.[22] Briefly, 200 μg of brain protein of control and ME7 scrapie-infected mice was dissolved in a rehydration buffer containing 8 mol/L urea, 2% CHAPS, 65 mmol/L dithiothreitol, 0.5% immobilized pH gradient (IPG) buffer (Bio-Rad), 40 mmol/L Tris-HCl, and 0.002% bromophenol blue. The brain homogenates were applied to the IPG Readystrip, 7 cm, pH 3 to 10 linear gradient (Bio-Rad). The IPG strips were rehydrated for 16 hours at 20°C using the PROTEAN isoelectric focusing cell (Bio-Rad) according to the manufacturer's instructions. Briefly, isoelectric focusing was conducted at 250 V for 15 minutes, linearly increased throughout 2 hours to a maximum of 4000 V, and then run to accumulate a total of 20,000 Vhours. The gel strips were equilibrated before second dimen-

sional electrophoresis for 15 minutes in 50 mmol/L Tris-HCl (pH 8.8) containing 6 mol/L urea, 30% glycerol, 2% sodium dodecyl sulfate, 0.002% bromophenol blue, and 80 mmol/L dithiothreitol or 0.025% iodoacetamide. The gel strips were then separated in 12% polyacrylamide gels to perform the second dimensional electrophoresis. The 2-DE gels were then exposed to Coomassie Brilliant Blue G-250 (CBBG-250) or silver staining. Duplicated 2-DE gels were also transferred on polyvinylidene difluoride membrane and then used for the detection of citrullinated proteins using an antibody to modified citrulline. The protein spots of immunoblotting-matched citrullinated proteins were subjected to in-gel trypsin digestion, and digested peptides were analyzed by matrix-assisted laser desorption/ionization-time of flight (MALDI-TOF) mass spectrometry (the Proteomics Service by Genomine, Pohang, Republic of Korea). The obtained peptide mass fingerprints spectra were analyzed by searching the Genomine local database and the National Centre for Biotechnology Information, nonredundant protein database with ProFound (*http://prowl.rockefeller.edu/prowl-cgi/profound.exe*).

Statistical Analysis

Quantitative results were expressed as means ± SEM. The probability of statistical differences between control and scrapie-infected groups was determined by a one-way analysis of variance test as indicated. Differences were considered significant at $P < 0.001$, $P < 0.01$, and $P < 0.05$.

Results

Increased Accumulation of Citrullinated Proteins in Various Brain Regions of Scrapie-Infected Mice

We first used Western blot analysis as described in the Materials and Methods to examine the citrullinated proteins from different brain regions of control and ME7 scrapie-infected mice. Total proteins were extracted from whole brains as well as from various dissected brain regions including cerebral cortex, hippocampus, striatum, cerebellum, and brain stem of control and scrapie-infected mice. In general, citrullinated proteins in most brain sections of scrapie-infected mice were markedly increased compared to controls (Figure 1, asterisks). In all brain regions, most bands from 10 kDa to 100 kDa were increased in scrapie. Those bands between 100 kDa and 150 kDa in whole brain, cerebellum, and brain stem were increased during scrapie infection, whereas no difference in citrullination was seen in other regions.

Next, we performed immunohistochemical staining of citrullinated proteins in different brain sections of control and scrapie-infected mice. As shown in Figure 2, citrullinated proteins (indicated by arrows) were more prominent in the scrapie-infected brains (Figure 2, F–J) than in control brains (Figure 2, A–E). These results correlated with the increased citrullinated proteins observed in scrapie-infected mice using Western blot analysis (Figure 1). We also observed similar results in the brains of 87V scrapie-infected mice (data not shown), indicating the occurrence of increased citrullination after infection is a general phenomenon.

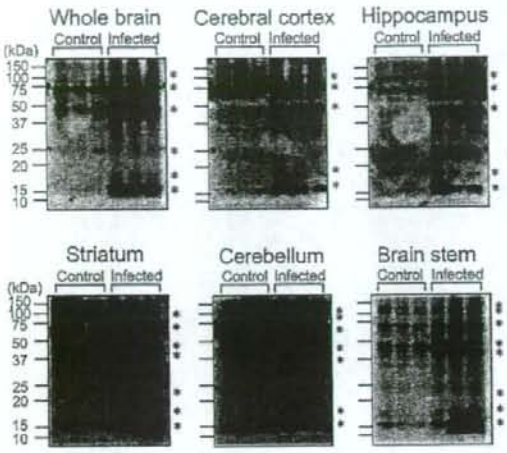

Figure 1. Detection of citrullinated proteins in brains from control and ME7 scrapie-infected mice. Whole brains and various brain sections of control (**lanes 1** to **3**) and ME7-infected mice (**lanes 4** to **6**) were homogenized, and then citrullinated proteins were detected by Western blot analysis using a polyclonal anti-modified citrulline antibody. Note that citrullinated proteins were increased in scrapie-infected regions compared to controls. Each lane shows the results for a homogenate obtained from brains of each individual mouse. **Asterisks** indicate the citrullinated proteins. These results are representative of at least three separate experiments.

Up-Regulation of PAD2 Expression in Various Brain Regions from Scrapie-Infected Mice

Posttranslational modification of protein arginine residues to citrulline is mediated by PAD2 enzyme in the brain. Therefore, we examined whether the expression levels of PAD2 in the brains are increased after ME7 scrapie infection. As can be seen in Figure 3A, the expression levels of PAD2 protein appeared to be increased in scrapie-infected mice in the following brain sections: cerebral cortex, hippocampus, striatum, and brain stem. However the expression level of PAD2 in cerebellum did not appear to be different between control and infected mice. Densitometric analysis of the gels showed that the relative intensity of the PAD2 bands was significantly higher in all sections of scrapie-infected brains compared to controls except in the cerebellum (Figure 3B).

In the next experiment, we measured expression levels of PAD2 mRNA in whole brains of both control and ME7 scrapie-infected mice using PAD2-specific primers as described in the Materials and Methods. As can be seen in Figure 3C, RT-PCR analysis showed increased PAD2

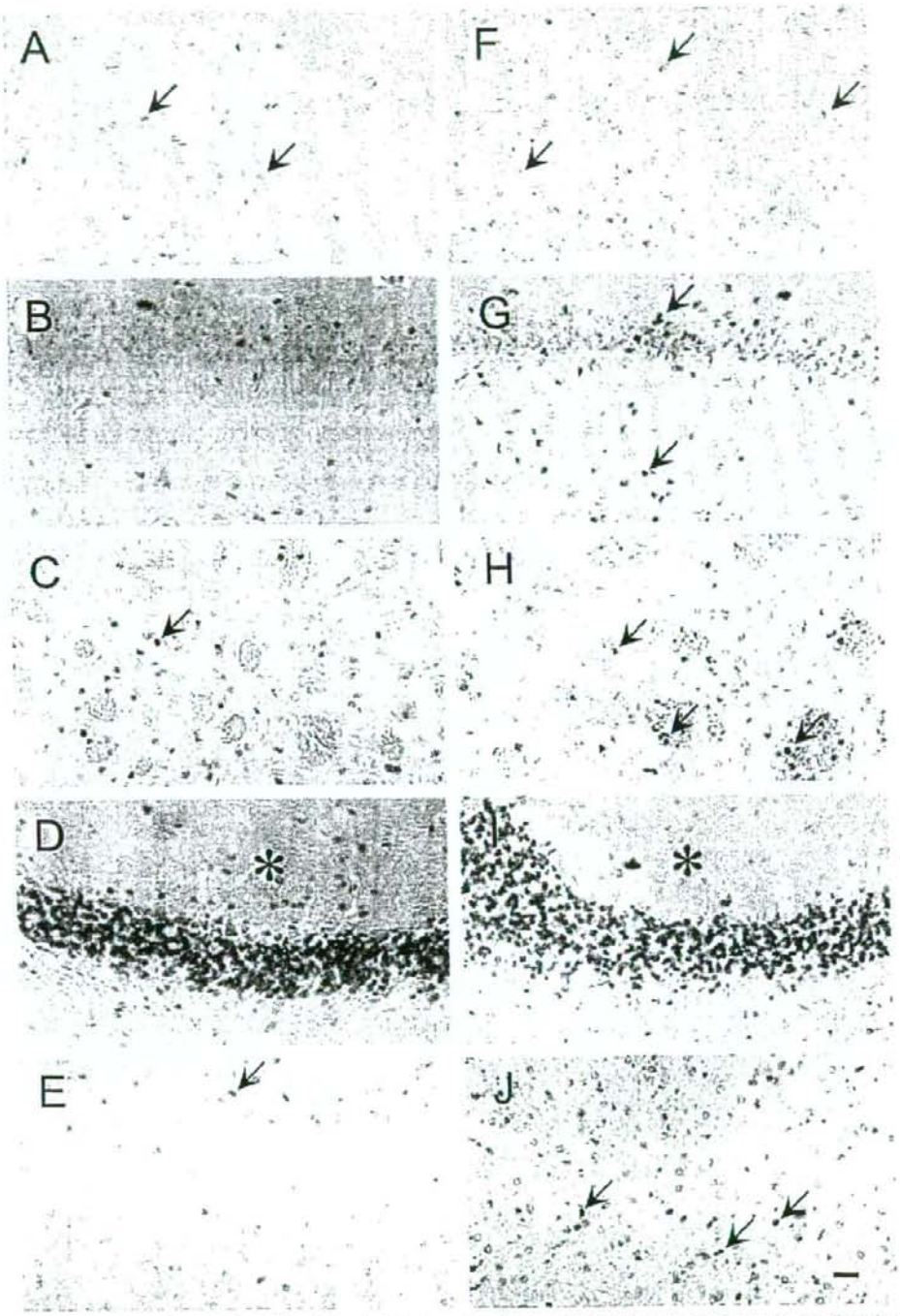

Figure 2. Immunohistochemical staining of citrullinated proteins in brain sections from control and ME7 scrapie-infected mice. Citrullinated proteins were detected in the brains of control (**A–E**) and scrapie-infected (**F–J**) mice at 160 days after inoculation. In the scrapie brain, citrullinated proteins (**arrows**) were more frequent than in control brains: cerebral cortex (**F**), hippocampus (**G**), striatum (**H**), cerebellum (**I**), and brain stem (**J**). **Asterisks** indicate the position of cerebellar molecular layer. Scale bar = 20 μm.

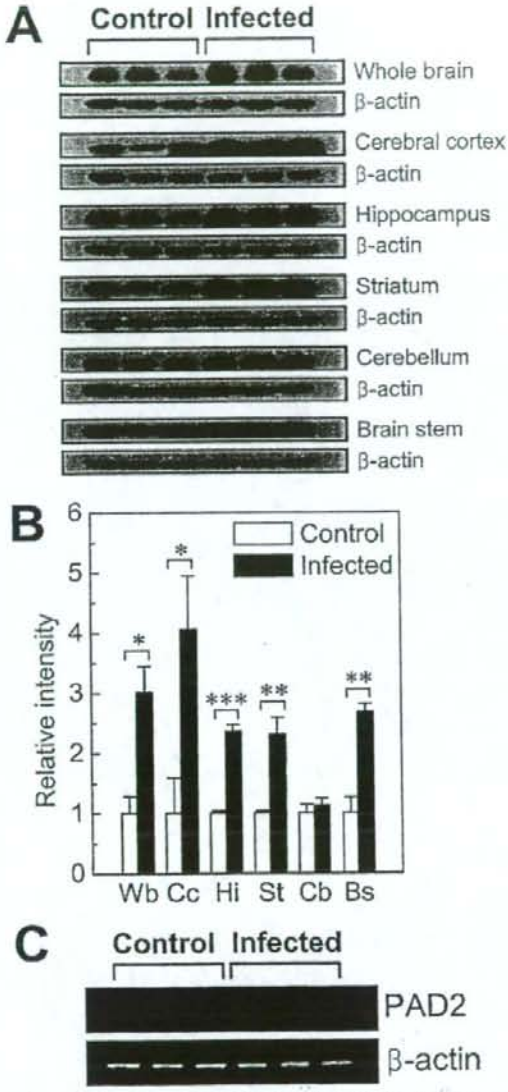

Figure 3. Comparison of expression level of PAD2 in brains from control and ME7 scrapie-infected mice. A: Expression level of PAD2 protein in whole brain and various brain sections of control and ME7-infected mice were analyzed by Western blot using a monoclonal anti-PAD2 antibody. Each lane shows the results for a homogenate obtained from dissected brain of each individual mouse. B: Densitometric analysis of bands in A normalized with β-actin. Wb, whole brain; Cc, cerebral cortex; Hi, hippocampus; St, striatum; Cb, cerebellum; Bs, brain stem. C: In whole brains, mRNA levels of PAD2 were analyzed by RT-PCR using three individuals of each group. Error bars represent SEM. $^{*}P < 0.05$, $^{**}P < 0.01$, $^{***}P < 0.001$.

mRNA in the whole brain of ME7 scrapie-infected mice compared to levels in controls. This result suggests that up-regulated expression of PAD2 protein seen in most brain regions is caused by an increase of gene expression in scrapie-infected mice.

Increased Immunofluorescence Staining of PAD2 in Reactive Astrocytes in Brains of Scrapie-Infected Mice

Next, to confirm the increased PAD2 expression and to determine the cellular localization of PAD2, immunohistochemical analysis was performed using various brain sections from control and scrapie-infected mice (Figure 4, A–E and F–J, respectively). In scrapie-infected brains, PAD2 immunoreactivity was more intense compared to control brains and these results correlated with the expression patterns of PAD2 protein in results of Western blot analysis (Figure 3A). According to previous reports, PAD2 is mainly expressed in glial cells such as astrocytes, oligodendrocytes, and microglial cells.[10–12] To further characterize the subcellular localization of PAD2, we performed double-immunofluorescence staining using GFAP, MBP, NeuN, and B4-isolectin as a marker for astrocytes, oligodendrocytes, neurons, and microglia, respectively. Interestingly, immunoreactivity was mainly observed in activated astrocytes in the brains of scrapie-infected mice. As can be seen in Figure 5, PAD2 was mainly co-localized with GFAP-positive astrocytes and in a few B4-isolectin-positive microglia, but not with MBP or NeuN. These data suggest that up-regulation of PAD2 expression in reactive astrocytes is responsible for the increased citrullinated proteins in the brains of scrapie-infected mice.

Elevated PAD2 Enzyme Activity in the Brains of Scrapie-Infected Mice

To investigate whether the increase in citrullinated proteins is attributable to higher levels of PAD2 enzyme activity and whether the increased PAD2 expression is correlated with its enzyme activity in scrapie-infected mice, we analyzed PAD2 enzyme activity in the brain homogenates of various sections from both control and ME7 scrapie-infected mice using benzoyl-L-arginine ethyl ester as a substrate as previously described.[9] PAD2 enzyme activity was significantly increased approximately twofold in whole brains as well as in hippocampus, striatum, and brain stem of scrapie-infected brains compared to controls (Figure 6A): whole brain [2.41-fold, control: 0.322 ± 0.052 (mean ± SEM, units); infected: 0.776 ± 0.039], hippocampus (2.19-fold, control: 0.342 ± 0.081; infected: 0.748 ± 0.120), striatum (2.48-fold, control: 0.256 ± 0.009; infected: 0.636 ± 0.082), and brain stem (1.99-fold, control: 0.589 ± 0.028; infected: 1.172 ± 0.055). The difference from controls was not significant in cerebral cortex (control: 0.193 ± 0.022; infected: 0.294 ± 0.032) or in cerebellum (control: 0.312 ± 0.041; infected: 0.419 ± 0.035). To determine whether the amount of PAD2 protein is associated with changes in enzyme activity, we compared the expression level of PAD2 protein in 50 μg of total protein from whole brain and from different brain regions of control and scrapie-infected mice. As shown in Figure 6B, the expression levels of PAD2 protein in cerebral cortex and in cerebellum were lower than other regions but still higher

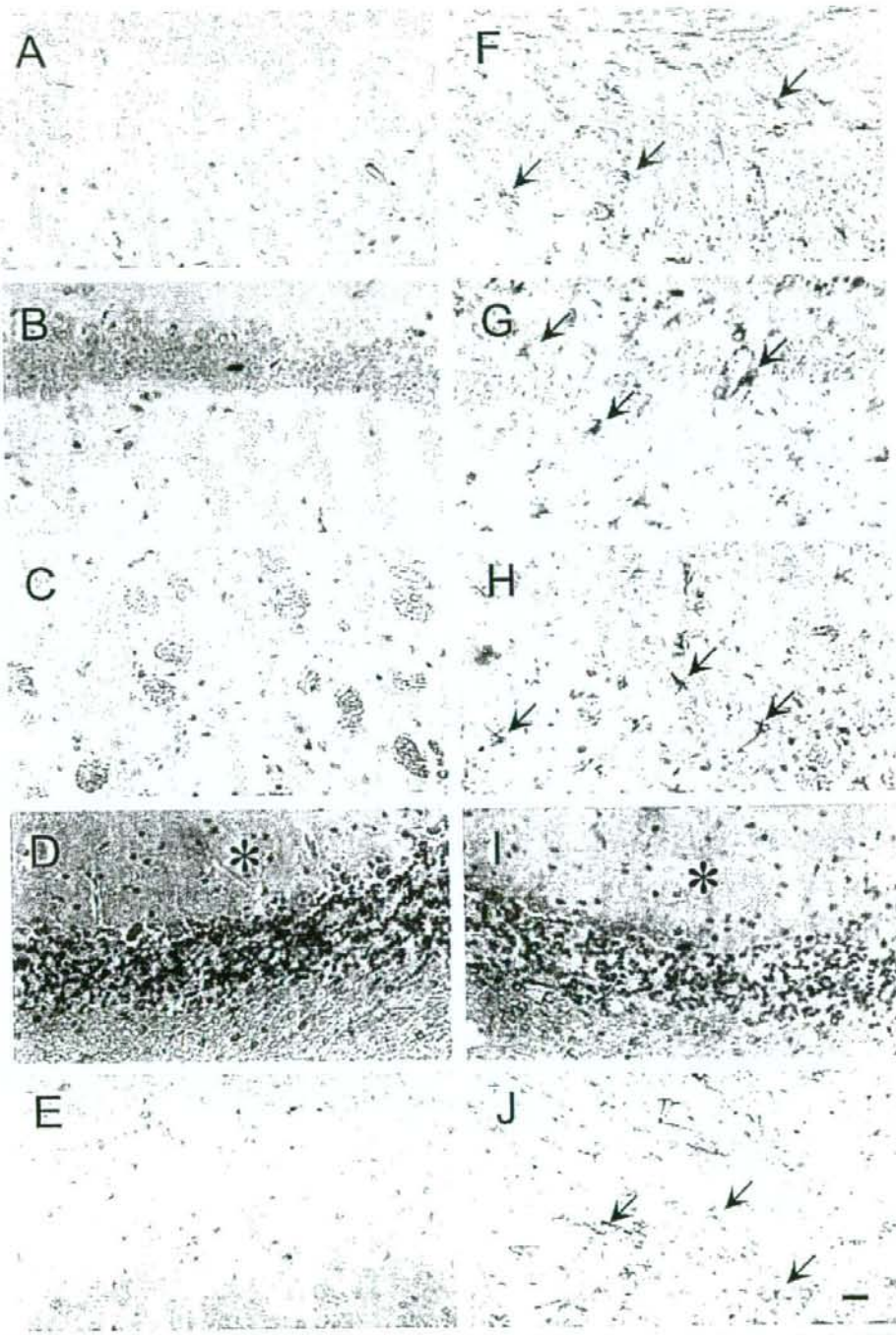

Figure 4. Expression of PAD2 in various brain sections. Immunohistochemical staining of PAD2 was performed using a monoclonal anti-PAD2 antibody in various brain sections from control (**A–E**) and ME7 scrapie-infected (**F–J**) mice. PAD2 was observed in dissected control and scrapie-infected brains at 160 days after inoculation with the ME7 scrapie strain. PAD2-positive cells were strongly immunostained in scrapie-infected brains and its immunoreactivity was observed in reactive astrocytes (**arrows**). **A** and **F**: Cerebral cortex; **B** and **G**: hippocampus; **C** and **H**: striatum; **D** and **I**: cerebellum; **E** and **J**: brain stem. **Asterisks** indicate the position of cerebellar molecular layer. Scale bar = 20 μm.

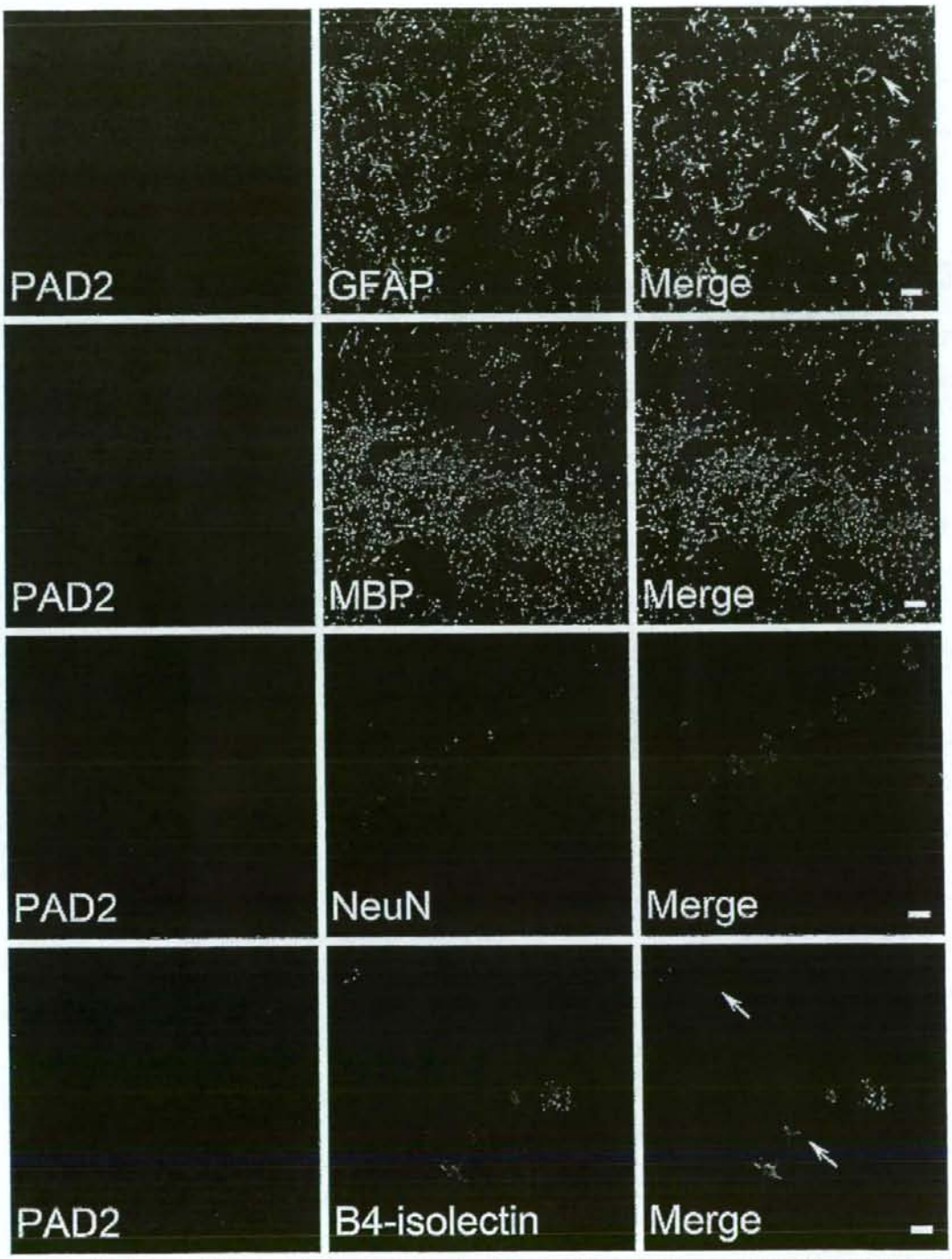

Figure 5. Cellular localization of PAD2 in scrapie-infected brains. The brain sections were doubly immunostained with anti-PAD2 and one of the following antibodies: astrocyte-specific GFAP, oligodendrocyte-specific MBP, neuron-specific NeuN, or microglia-specific B4-isolectin antibodies. Slides were examined under confocal laser-scanning microscopy. Note that PAD2-positive cells were strongly co-localized in cells positive for GFAP (**arrows**) with very few B4-isolectin-positive microglia (**arrows**). Scale bars = 20 μm.